

# On jet structure in heavy ion collisions

I. P. Lokhtin<sup>a</sup>, A. A. Alkin, A. M. Snigirev

Skobeltsyn Institute of Nuclear Physics, Lomonosov Moscow State University, Moscow, Russia

Received: 6 October 2014 / Accepted: 30 July 2015 / Published online: 25 September 2015  
© The Author(s) 2015. This article is published with open access at Springerlink.com

**Abstract** The LHC data on jet fragmentation function and jet shapes in PbPb collisions at center-of-mass energy 2.76 TeV per nucleon pair are analyzed and interpreted in the frameworks of PYthia QUENched (PYQUEN) jet quenching model. A specific modification of longitudinal and radial jet profiles in most central PbPb collisions as compared with pp data is close to that obtained with PYQUEN simulations, taking into account wide-angle radiative and collisional partonic energy losses. The contribution of radiative and collisional loss to the medium-modified intra-jet structure is estimated.

## 1 Introduction

Studying the modification of jets as they are formed from energetic partons propagating through the hot and dense medium created in ultrarelativistic heavy ion collisions is a particularly useful tool for probing the produced matter's properties. The energy loss of jet partons in a deconfined medium, a quark–gluon plasma, is predicted to be much stronger than in cold nuclear matter, and this leads to the so-called “jet quenching” effect (see, e.g., the reviews in [1–7] and references therein). Indirectly jet quenching was observed for the first time at RHIC experiments via measurements of inclusive high- $p_T$  hadron production in gold–gold collisions at center-of-mass energy  $\sqrt{s_{NN}} = 200$  GeV. It was manifested as the suppression of overall high- $p_T$  hadron rates and back-to-back dihadron azimuthal correlations (including the specific azimuthal angle dependence of the effect with respect to the event plane). A summary of experimental results at RHIC can be found in [8–11].

The lead–lead collision energy at LHC,  $\sqrt{s_{NN}} = 2.76$  TeV, is a factor of  $\sim 14$  larger than that in RHIC, and it thereby allows one to probe new frontiers of super-hot quark–gluon matter. The analysis of high statistics samples of fully reconstructed jets becomes possible. The results of jet analyses

of 2010 and 2011 PbPb data obtained by three LHC experiments, ALICE, ATLAS, and CMS, are summarized e.g. in the review in [12]. The first direct evidence of jet quenching has been observed as a large, centrality-dependent, imbalance in dijet transverse energy [13,14]. It has been found using missing  $p_T$  techniques that the jet energy loss spreads over low transverse momenta and large angles [14]. Then the jet momentum dependence of the dijet imbalance has been studied in detail [15]. A significant transverse energy imbalance has been observed for photon+jet production in PbPb events [16]. Another direct manifestation of jet quenching is the inclusive jet suppression in central PbPb collisions compared to peripheral events [17,18] and to proton–proton interactions [19]. The azimuthal angle dependence of such a suppression has also been measured [20]. A similar level of suppression as for inclusive jets is seen for jets from b-quark fragmentation [21]. In contrast to PbPb collisions, proton–lead data from LHC do not show jet quenching [22].

A number of theoretical calculations and Monte-Carlo simulations were attempted to reproduce some of basic features of jet quenching pattern at LHC (dijet and photon+jet imbalance, nuclear modification factors for jets and high- $p_T$  hadrons), and to extract in such a way information as regards medium properties and partonic energy loss mechanisms [23–42]. The observable that allows for a more precise comparison between the data and theoretical models of jet quenching to be done is the internal jet structure. The recently published experimental data on the medium-modified jet structure include the measurement of jet shapes (radial profile) [43] and the jet fragmentation function (longitudinal profile) [44,45]. It was suggested in [46] that it could also be of interest to study moments of jet fragmentation function.

In the present paper, the LHC data on the jet fragmentation function and jet shapes in PbPb collisions are analyzed and interpreted in the frameworks of the PYthia QUENched (PYQUEN) partonic energy loss model [47]. In [27,28] this model was applied to an analysis of the dijet energy asymmetry and the nuclear modification factor of inclusive hadrons.

<sup>a</sup>e-mail: igor@lav01.simp.msu.ru

## 2 PYQUEN model

PYQUEN is one of the first Monte-Carlo models of jet quenching [47]. PYQUEN was constructed as a modification of jet events obtained with the generator of hadron–hadron interactions PYTHIA\_6.4 [48]. The details of the physics model and simulation procedure used can be found in the original paper [47]. The main features of the model are listed below as follows.

The approach describing the multiple scattering of hard partons relies on the accumulated energy loss via gluon radiation, which is associated with each parton scattering in a hot matter. It also includes the interference effect in gluon emission with a finite formation time using the modified radiation spectrum  $dE/dl$  as a function of the decreasing temperature  $T$ . The basic kinetic integral equation for the partonic energy loss  $\Delta E$  as a function of initial energy  $E$  and path length  $L$  has the form

$$\Delta E(L, E) = \int_0^L dl \frac{dP(l)}{dl} \lambda(l) \frac{dE(l, E)}{dl}, \tag{1}$$

$$\frac{dP(l)}{dl} = \frac{1}{\lambda(l)} \exp(-l/\lambda(l)),$$

where  $l$  is the current transverse coordinate of a parton,  $dP/dl$  is the scattering probability density,  $dE/dl$  is the energy loss per unit length,  $\lambda = 1/(\sigma\rho)$  is the in-medium mean free path,  $\rho \propto T^3$  is the medium density at the temperature  $T$ ,  $\sigma$  is the integral cross section for the parton interaction in the medium.

The model takes into account the radiative and collisional energy loss of hard partons in a longitudinally expanding quark–gluon fluid, as well as the realistic nuclear geometry. The radiative energy loss is treated in the framework of the BDMPS model [49–51]:

$$\frac{dE^{\text{rad}}}{dl} = \frac{2\alpha_s(\mu_D^2)C_R}{\pi L} \int_{\mu_D^2\lambda_g}^E d\omega \left[ 1 - y + \frac{y^2}{2} \right] \ln |\cos(\omega_1 \tau_1)|,$$

$$\omega_1 = \sqrt{i \left( 1 - y + \frac{C_R}{3} y^2 \right) \bar{k} \ln \frac{16}{\bar{k}}}, \quad \bar{k} = \frac{\mu_D^2 \lambda_g}{\omega(1-y)}, \tag{2}$$

where  $\tau_1 = L/(2\lambda_g)$ ,  $y = \omega/E$  is the fraction of the hard parton energy carried away by the radiated gluon,  $\alpha_s$  is the QCD running coupling constant for  $N_f$  active quark flavors,  $C_R = 4/3$  is the quark color factor, and  $\mu_D$  is the Debye screening mass. A similar expression for the gluon jet can be obtained by setting  $C_R = 3$  and properly changing the factor in the square brackets in (2) [50]. The simple generalization to the radiative energy loss of the massive quark case uses the “dead-cone” approximation [52].

The collisional energy loss due to elastic scatterings is calculated in the high-momentum transfer limit [53–55]:

$$\frac{dE^{\text{col}}}{dl} = \frac{1}{4T\lambda\sigma} \int_{\mu_D^2}^{t_{\text{max}}} dt \frac{d\sigma}{dt} t, \tag{3}$$

where the dominant contribution to the differential scattering cross section is

$$\frac{d\sigma}{dt} \cong C \frac{2\pi\alpha_s^2(t)}{t^2} \frac{E^2}{E^2 - m_p^2} \tag{4}$$

for the scattering of a hard parton with energy  $E$  and mass  $m_p$  off the “thermal” parton with energy (or effective mass)  $m_0 \sim 3T \ll E$ . Here  $C = 9/4, 1, 4/9$  for the  $gg, gq,$  and  $qq$  scatterings, respectively. The integrated cross section  $\sigma$  is regularized by the Debye screening mass squared  $\mu_D^2(T) \simeq 4\pi\alpha_s T^2(1 + N_f/6)$ . The maximum momentum transfer is  $t_{\text{max}} = [s - (m_p + m_0)^2][s - (m_p - m_0)^2]/s$  where  $s = 2m_0E + m_0^2 + m_p^2$ .

The medium where partonic rescattering occurs is considered as a boost-invariant longitudinally expanding perfect quark–gluon fluid, and the partons as being produced on a hyper-surface of equal proper times  $\tau$  [56]. Then the proper time dependence of the temperature  $T$ , energy density  $\varepsilon$ , and number density  $\rho$  gets the form

$$\varepsilon(\tau) = \varepsilon_0 \left( \frac{\tau_0}{\tau} \right)^{4/3}, \quad T(\tau) = T_0 \left( \frac{\tau_0}{\tau} \right)^{1/3}, \quad \rho(\tau) = \rho_0 \frac{\tau_0}{\tau}. \tag{5}$$

In principle, other scenarios of the space-time evolution of quark–gluon matter can be considered within the PYQUEN model [47]. For example, the presence of fluid viscosity slows down the cooling rate, i.e., in fact the effective temperature gets higher as compared with the perfect fluid case. At the same time, the influence of the transverse expansion of the medium on the parton rescattering intensity is practically inessential for high initial temperatures  $T_0^{\text{max}}$ .

The strength of the partonic energy loss in PYQUEN is determined mainly by the initial maximal temperature  $T_0^{\text{max}}$  of the hot fireball in central PbPb collisions, which is achieved in the center of the nuclear overlapping area at mid-rapidity. The transverse energy density in each point inside the nuclear overlapping zone is supposed to be proportional to the impact-parameter dependent product of two nuclear thickness functions  $T_A$  in this point:

$$\varepsilon(r_1, r_2) \propto T_A(r_1)T_A(r_2), \tag{6}$$

where  $r_{1,2}$  are the transverse distances between the centers of colliding nuclei and the parton production vertex. The rapidity dependent spreading of the initial energy density around mid-rapidity  $y = 0$  is taken in the Gaussian-like form. The partonic energy loss depends also on the proper

time  $\tau_0$  of matter formation and the number  $N_f$  of active flavors in the medium. Note that the variation of the  $\tau_0$  value within its reasonable range has a rather moderate influence on the strength of the partonic energy loss. The jet quenching gets stronger at larger  $\tau_0$  due to a slower medium cooling, which implies the jet partons spend more time in the hottest regions, and as a result the rescattering intensity somewhat increases [27].

Another important ingredient of the model is the angular spectrum of the medium-induced radiation. There is a number of recent theoretical achievements related to this subject (see, e.g., [34, 57–60]). Nevertheless to the best of our knowledge there is no unique well-defined angular spectrum of emitted gluons in the current literature to be implemented in Monte-Carlo models unambiguously. This is one of the main reasons leading to various approaches to modeling of the medium-induced partonic energy loss in the existing event generators. Since the detailed Monte-Carlo treatment of the angular spectrum of medium-induced radiation is rather sophisticated and ambiguously determined, the simple parameterizations of the gluon distribution over the emission angle  $\theta$  are used within PYQUEN, to get some notion about possible effects related to the angular structure and to illustrate our interpretation of the data. There are two basic limiting options in the model. The first one is the “small-angle” radiation,

$$\frac{dN^g}{d\theta} \propto \sin \theta \exp\left(-\frac{(\theta - \theta_0)^2}{2\theta_0^2}\right), \quad (7)$$

where  $\theta_0 \sim 5^\circ$  is the typical angle of the coherent gluon radiation as estimated in [61]. This scenario results in predictions very close to those obtained under the assumption that all gluons are emitted collinearly (along the direction of motion of the radiating particle). The second option is the “wide-angle” radiation,

$$\frac{dN^g}{d\theta} \propto 1/\theta, \quad (8)$$

which is similar to the angular spectrum of parton showering in a vacuum without coherent effects [62]. The physical meaning of wide-angle radiation could be the presence of intensive secondary rescatterings of in-medium emitted gluons [24]. It may result in destroying the small-angle (BDMPS-like) coherence emission and significant broadening of the gluon emission angular spectrum. This scenario allows us to estimate the effects of radiation outside the typical jet cone. The collisional energy loss in PYQUEN is always an “out-of-cone” loss. Energy thus lost is considered as “absorbed” by the medium, because the major part of “thermal” particles knocked out of the hot matter by elastic rescatterings fly outside the typical jet cone [61].

The event-by-event Monte-Carlo simulation procedure in PYQUEN includes three main steps: the generation of ini-

tial parton spectra with PYTHIA and production vertexes at the given impact parameter; the rescattering-by-rescattering passage of each jet parton through a dense zone accompanied with gluon radiation and collisional energy loss; the final hadronization for jet partons and in-medium emitted gluons according to the standard Lund string scheme implemented in PYTHIA.

### 3 Results

The PYQUEN model was applied to simulate medium-modified inclusive jet production at an energy  $\sqrt{s_{\text{NN}}} = 2.76$  TeV for different PbPb centralities. The radiative and collisional energy losses were taken into account. Two options for the angular spectrum of the gluon radiation were considered: wide- and small-angle radiative loss. Hereafter let us call these options “Scenario *W*” and “Scenario *S*”, respectively. The discrimination between these two ultimate scenarios when analyzing various jet characteristics seems particularly interesting, because it allows one to get some notion as regards the possible effects related to the angular structure of the medium-induced partonic energy loss. “Scenario *S*” results in very close predictions to those obtained under the assumption that gluons are emitted collinearly, while “Scenario *W*” is useful to estimate the effects of the radiation outside the typical jet cone. At the same time a specific form of angular spectrum is not crucial for these two extreme cases; only a part of the energy loss outside the typical jet cone is significant for the effects under consideration.

The PYQUEN parameter values  $T_0^{\text{max}} = 1$  GeV,  $\tau_0 = 0.1$  fm/c and  $N_f = 0$  (gluon-dominated plasma) were used for our simulations. Such parameter settings allow the model to reproduce the LHC data on dijet transverse energy imbalance and nuclear modification factors of inclusive hadrons as wide-angle radiative and collisional energy losses are taken into account [27, 28]. PYTHIA tune Pro-Q20 was utilized.

In the current paper we do not intend to do a complete “apples to apples” comparison of the model results with the data. Such a kind of comparison for jet observables should contain a full (or fast) simulation of the detector responses, which has to work within the experiment’s software suite and it certainly cannot be done in the context of a phenomenological paper. However, we try to take into account the basic experimental effects (affecting the jet observables) in some simplified but reasonable ways. In order to include a jet reconstruction on the calorimetric level in our simulation, we apply the iterative cluster finding algorithm PYCELL implemented in PYTHIA [48]. The final state jets within the cone size  $R^{\text{jet}} = \sqrt{\Delta\varphi^2 + \Delta\eta^2} = 0.3$  with transverse energy  $E_T^{\text{jet}} > 100$  GeV and pseudorapidity  $0.3 < |\eta^{\text{jet}}| < 2$  were considered. The numerical results were compared with the CMS data on the modification factors for the jet shapes [43]

and the jet fragmentation function [44] using the same kinematic cuts as in the experiment. Note that the data have been obtained in a more complicated way, using the anti- $k_T$  algorithm [63], utilizing so-called particle-flow objects, which combine tracking and calorimetric information. However, we assume that the physical observables should be stable for different reasonable algorithms. For example, in [14] the calorimeter-based iterative cone algorithm was applied as a basic option for jet reconstruction, while the anti- $k_T$  algorithm based on particle flow objects was used for a cross-check of the results. Good agreement between the results obtained with the two algorithms has been found.

Another simplification in our simulation is not taking into account the high multiplicity background. The correct performance of the jet reconstruction algorithms and the background subtraction procedure is checked and verified in any such experimental analysis (including ones discussed in the current paper). So the measured physical observables are supposed to be stable with respect to the background fluctuations. Since the attempt to reproduce the jet analysis procedure within the model in exactly the same way as in the experiment would require huge extra efforts without crucial influence on the results obtained, and we believe that our simulation of experimental effects is enough to support our main physical conclusions.

At first we have checked that the overall suppression of inclusive jet rates for 10 % of most central PbPb events as compared to the corresponding pp collisions (scaled to the number of binary nucleon–nucleon collisions) almost does not depend on  $E_T^{\text{jet}}$  and is found on the level  $R_{AA}^{\text{jet}} \sim 0.5 \div 0.55$  for “Scenario  $S$ ” and  $R_{AA}^{\text{jet}} \sim 0.4 \div 0.45$  for “Scenario  $W$ ”. Both results are close to the ATLAS measurements of the jet suppression factor [17, 19] within the statistical and systematic uncertainties of the data. Since no qualitative difference between “Scenario  $W$ ” and “Scenario  $S$ ” is seen for the energy dependence of  $R_{AA}^{\text{jet}}$  (only a numerical difference  $\sim 20$  % independently of  $E_T^{\text{jet}}$ ), making unambiguous conclusions in favor of either scenario based on  $R_{AA}^{\text{jet}}$  measurements would be rather difficult. Our explanation for this is as follows. The naive expectation is that small-angle radiation will, in the first place, soften the particle energy distributions inside the jet and increase the multiplicity of secondary particles, but it (almost) will not affect the total jet energy. In such a case jet suppression could be significantly less pronounced than the one for wide-angle radiation. However, the inevitable feature of any jet reconstruction algorithm is the separation of high and low transverse momentum particles (clusters) to treat them as extracted signal and subtracted background, respectively. Thus softening of the particle distribution inside the jet effectively results in a loss of jet energy, and the difference between the two scenarios for the jet suppression factors becomes not so pronounced.

Then we consider the jet internal structure. The radial jet profile may be characterized by the distribution of the transverse momentum inside the jet cone:

$$\rho(r) = \frac{1}{\delta r} \frac{1}{N_{\text{jet}}} \sum_{\text{jets}} \frac{p_T(r - \delta r/2, r + \delta r/2)}{E_T^{\text{jet}}}, \quad (9)$$

where  $r = \sqrt{(\eta - \eta_{\text{jet}})^2 + (\varphi - \varphi_{\text{jet}})^2} \leq R^{\text{jet}}$  is the radial distance from the jet particle to the jet axis, defined by the coordinates  $\eta_{\text{jet}}$  and  $\varphi_{\text{jet}}$ . Following the CMS analysis procedure [43] the jet cone was divided into six bins with radial width  $\delta r = 0.05$ , and the transverse momentum of all charged particles with  $p_T > 1$  GeV/ $c$  in each radial bin was summed to obtain the fraction of the total jet  $p_T$  carried by these particles. Then the results were averaged over the total number of found jets,  $N_{\text{jet}}$ .

The longitudinal jet profile usually is characterized by the jet fragmentation function  $D(z)$  defined as the probability for a jet particle to carry a fraction  $z$  of the jet transverse energy. Often the jet fragmentation function is measured in terms of the variable  $\xi = \ln(1/z) = \ln(E_T^{\text{jet}}/p_T)$ , and it is normalized to the total number of jets,  $N_{\text{jet}}$ . The charged particles with  $p_T > 1$  GeV/ $c$  in a jet cone were selected for the analysis [44].

Figure 1 shows the jet shape nuclear modification factors,  $\rho(r)(\text{PbPb})/\rho(r)(\text{pp})$ , for four centralities of PbPb collisions. The specific modification of the radial jet profile in most central collisions due to a redistribution of the jet energy inside the cone is observed. It includes the excess at large radii, the suppression at intermediate radii, and an unchanged (or slightly enhanced) jet core. PYQUEN (“Scenario  $W$ ”) produces a similar modification close to the data (within the experimental uncertainties). At the same time PYQUEN (“Scenario  $S$ ”) gives a qualitatively very different result, such as an excess at large and intermediate radii, and suppression for the jet core. A similar situation appears for the jet fragmentation function (Fig. 2). The same prominent features for the ratio of the PbPb jet fragmentation function to its pp reference seen in the data and in the PYQUEN (“Scenario  $W$ ”): the excess at low  $p_T$  (large  $\xi$ ), the suppression at intermediate  $p_T$  ( $\xi$ ), and the indication of some enhancement at high  $p_T$  (small  $\xi$ , the domain of the leading particles). Note that recent ATLAS data on the jet fragmentation function [45] support the presence of an excess at high  $p_T$  with more confidence (but this comparison was done with respect to peripheral PbPb events). As with jet shapes, PYQUEN (“Scenario  $S$ ”) fails to reproduce measured jet fragmentation functions, providing the suppression at high  $p_T$ .

In order to analyze the relative contribution of the wide-angle radiative and collisional energy losses to the medium-modified intra-jet structure, two additional PYQUEN options were considered: wide-angle radiative loss only (without collisional loss) and collisional loss only (without radiative loss).

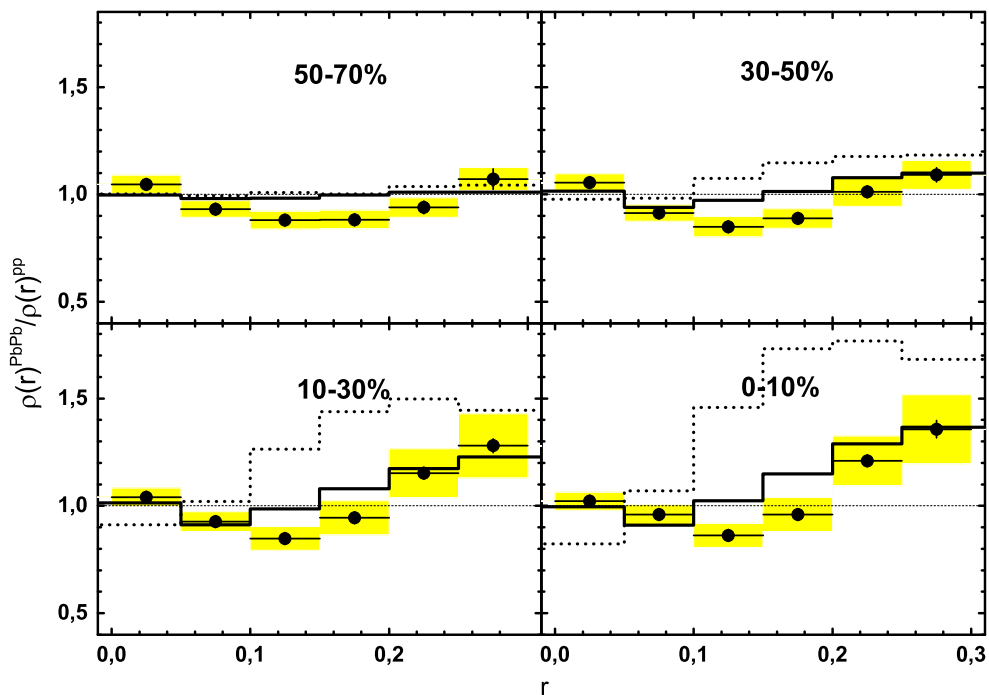


**Fig. 1** Jet shape nuclear modification factors as a function of distance from the jet axis in PbPb collisions (four centralities) at  $\sqrt{s_{NN}} = 2.76$  TeV for inclusive jets with  $E_T^{\text{jet}} > 100$  GeV and pseudorapidity  $0.3 < |\eta^{\text{jet}}| < 2$ . The charged particles with  $p_T > 1$  GeV/c in a jet cone  $R = 0.3$  are included. The closed circles are CMS data [43], the error

bars show the statistical uncertainties, and the boxes show the systematic errors. The solid and dashed histograms are simulated PYQUEN events for “Scenario W” (wide-angle radiative plus collisional energy loss) and by “Scenario S” (small-angle radiative plus collisional energy loss), respectively

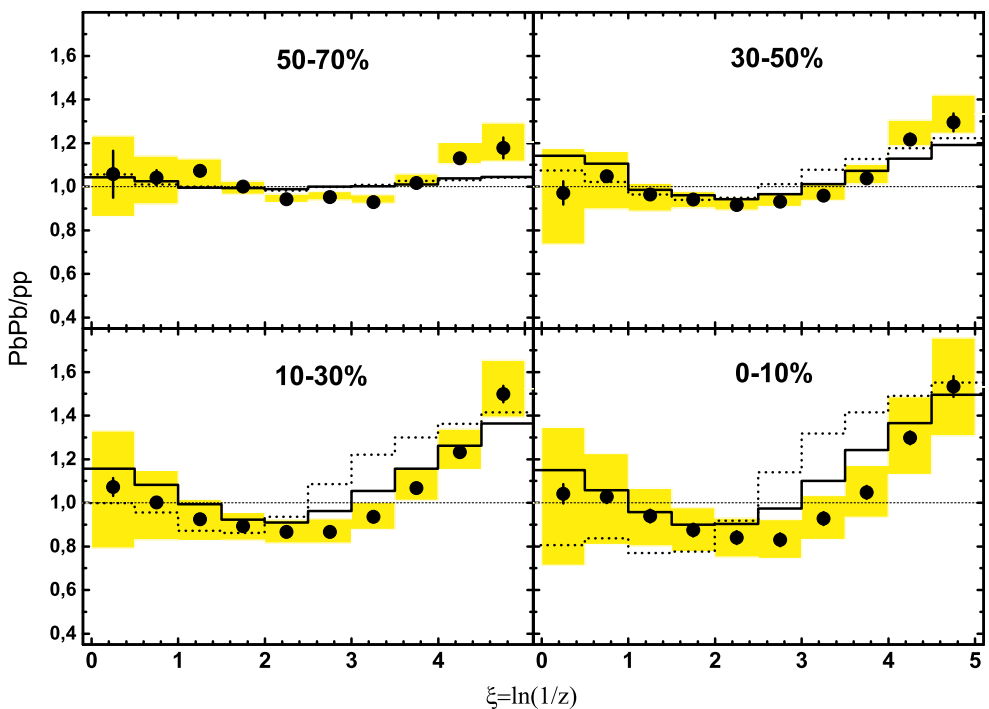


**Fig. 2** The ratio of jet fragmentation function in PbPb collisions (four centralities) to its pp reference at  $\sqrt{s_{NN}} = 2.76$  TeV for inclusive jets with  $100 < E_T^{\text{jet}} < 300$  GeV and pseudorapidity  $0.3 < |\eta^{\text{jet}}| < 2$ . The charged particles with  $p_T > 1$  GeV/c in a jet cone  $R = 0.3$  are included. The closed circles are CMS data [44], the error bars show the statistical

uncertainties, and the boxes show the systematic errors. The solid and dashed histograms are the simulated PYQUEN events for “Scenario W” (wide-angle radiative plus collisional energy loss) and “Scenario S” (small-angle radiative plus collisional energy loss), respectively

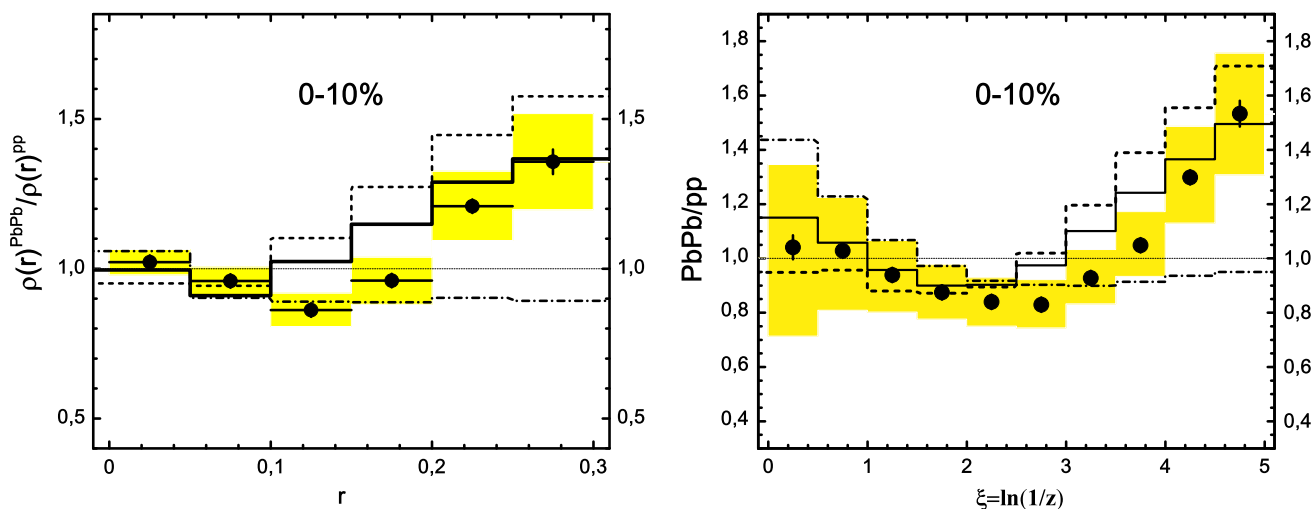


**Fig. 3** Jet shape nuclear modification factor as a function of distance from the jet axis in PbPb collisions (*left*) and the ratio of jet fragmentation function in PbPb collisions to its pp reference (*right*) at  $\sqrt{s_{\text{NN}}} = 2.76$  TeV (0–10% centrality) for inclusive jets with  $E_{\text{T}}^{\text{jet}} > 100$  GeV and pseudorapidity  $0.3 < |\eta^{\text{jet}}| < 2$ . The charged particles with  $p_{\text{T}} > 1$  GeV/c in a jet cone  $R = 0.3$  are included. The

*closed circles* are CMS data [43,44], the *error bars* show the statistical uncertainties, and the *boxes* show the systematic errors. The *solid*, *dashed* and *dash-dotted histograms* are simulated PYQUEN events for “Scenario W” (wide-angle radiative plus collisional energy loss), scenario “wide-angle radiative loss only” and scenario “collisional energy loss only”, respectively

The corresponding results for the jet shape nuclear modification factors and jet fragmentation function are shown on Fig. 3 for 10% of the most central PbPb collisions. As expected, the contribution from the wide-angle radiative energy loss dominates. So the option “wide-angle radiative loss only” provides a much stronger modification of the jet profile than the modification obtained for the option “collisional loss only”. With all this, the scenario with wide-angle radiative loss alone cannot match the data well, so taking into account both contributions is necessary. Note that the relative weight between both contributions is not regulated specially in the model, but implicitly it is determined by the physical assumptions when calculating the radiative and collisional energy losses (Eqs. (2) and (3)) and by the settled model parameter values (mostly the initial maximal temperature  $T_0^{\text{max}}$ ).

#### 4 Discussion

Let us discuss now the possible origin of such a specific medium-modified jet structure. In-medium emitted gluons are softer than initial jet partons, and fly at some angle with respect to the parent parton direction. Thus it is quite expectable that such “additional” gluons contribute to an excess of hadron multiplicity at low transverse momenta and jet radial broadening. On the other hand, the energy loss of the initial jet partons reduces a number of hadrons at high and intermediate transverse momenta, such hadrons being strongly correlated with a jet axis. Then at first glance it should result in the suppression of hadron multiplicities in a

jet core and at high  $p_{\text{T}}$ , which contradicts the data. However, in fact the medium-modified jet structure at intermediate and high  $p_{\text{T}}$  is determined by the interplay of two effects. The first one is radial broadening and longitudinal softening due to rescatterings and energy loss of the jet partons. The second one is shifting down the jet energy due to the “out-of-cone” energy loss. The energy loss of a jet as a whole results in the difference between the “initial” (non-modified) and final jet energies. Since more energetic jets initially are more collimated and the particle  $p_{\text{T}}$ -spectrum in such jets is harder, the two above effects enter into competition. If the contribution of the wide-angle partonic energy loss to the total loss is large enough, the decrease in the yield of jet particles at high  $p_{\text{T}}$  and the broadening of the jet core can be compensated by significant jet energy “rescaling” and converted into an increase in the particle yield and (almost) an unmodified radial profile at small radii. Such a specific behavior of the medium-modified jet fragmentation function at high  $p_{\text{T}}$  has been predicted some years ago in [64] (see also subsection 6.16.2 in [65]). The influence of the measured jet fragmentation functions by the enhanced quark-to-gluon jet fraction can also be important [12].

Note that the parameterizations (7) and (8) for the gluon angular spectrum may be rather easily can account for all the features of the intra-jet activity in the data, our treatment of calorimetric jet finding, moreover, being inevitably simplified as compared with the realistic experimental procedure. However, it does not affect the main physical message originating from the present studies: the data support the supposition that the intensive wide-angle (out-of-jet-cone) partonic energy loss occurs in most central PbPb collisions, while the

scenario with small-angle loss seems to be inconsistent with the data. This interpretation is also in agreement with the results of our previous model analysis of a medium-induced imbalance in the dijet transverse energy [27]. As we already have mentioned above, a specific form of angular spectrum is not so important here, only a part of the energy loss outside the typical jet cone affects this kind of jet observables. For example, in [64] we analyzed the relation between the in-medium softening jet fragmentation function and the suppression of the jet rates due to the energy loss outside the jet cone without using the explicit form of the angular spectrum at all. Within the current study, we have found that increasing the parameter  $\theta_0$  in (7) by a factor  $\sim 3$  results in a similar modification of the longitudinal and radial jet profiles to “Scenario W”. Thus since the large rise in typical radiation angle and its smearing in the parameterization (7) effectively reproduces the wide-angle radiation case (8), a particular form of angular spectrum cannot be verified unambiguously within our simulation.

Finally, we would like to refer to some other recent theoretical calculations for jet structure observables in PbPb collisions at the LHC. The jet fragmentation function was calculated and compared with the data in Refs. [34, 42, 66, 67]. The JEWEL event generator [34] and the hybrid strong/weak coupling jet quenching model [42] are successful in describing the basic trends seen in the data excepting the low- $p_T$  region. Hardening of the fragmentation function at high  $p_T$  in these models is a consequence of the depletion of softer jet particles. An effective 1 + 1 dimensional quasi-Abelian model [66] is able to reproduce the low and intermediate  $p_T$ -region, and it predicts an unmodified fragmentation at high  $p_T$ . The jet fragmentation function [67] and jet shapes [58] were studied also with YaJEM event generator. It has been found that the YaJEM results are qualitatively consistent with measurements of the jet fragmentation function, while a simulated jet broadening seems to be significantly stronger than in the data.

## 5 Conclusion

A modification of the jet fragmentation function and jet shapes in PbPb collisions at  $\sqrt{s_{NN}} = 2.76$  TeV with respect to the corresponding pp data has been analyzed in the frameworks of the PYQUEN partonic energy loss model. The PYQUEN simulations with wide-angle radiative and collisional energy losses provide specific medium-induced modifications of the longitudinal and radial jet profiles in the most central collisions, which are close to the experimentally observed ones. In spite of the contribution from wide-angle radiative loss to the medium-modified intra-jet structure being found to dominate, taking into account collisional loss is also necessary to match the data. Some excess in the

yield of jet particles at high  $p_T$  and an (almost) unmodified jet core may be explained by significant shifting down the jet energy due to an “out-of-cone” energy loss. At the same time, the scenario with small-angle energy loss does not reproduce this effect, and so it seems to be inconsistent with the data. We suppose that when the contribution of wide-angle energy loss to the total loss becomes large enough, the decrease in the yield of jet particles at high transverse momenta and the broadening of a jet core is compensated by a significant jet energy “rescaling” and converted into an increase in the particle yield and an (almost) unmodified radial profile at small radii. Such a rescaling is not possible if the small-angular loss is the dominant source of energy loss.

Together with other jet observables, the medium-modified jet structure seen in most central PbPb collisions at the LHC supports the presence of intensive wide-angle partonic energy loss, and this can put strong constraints on the theoretical models of jet quenching. Future LHC data collected at increased energy and luminosity are expected to yield more precise measurements of various jet characteristics in heavy ion collisions. This will allow us to study the jet quenching mechanisms and properties of hot deconfined matter in more detail.

**Acknowledgments** Discussions with M. Spousta and A. I. Demianov are gratefully acknowledged. We thank our colleagues from CMS collaboration for fruitful cooperation. This work was supported by Russian Scientific Fund (Grant 14-12-00110).

**Open Access** This article is distributed under the terms of the Creative Commons Attribution 4.0 International License (<http://creativecommons.org/licenses/by/4.0/>), which permits unrestricted use, distribution, and reproduction in any medium, provided you give appropriate credit to the original author(s) and the source, provide a link to the Creative Commons license, and indicate if changes were made. Funded by SCOAP<sup>3</sup>.

## References

1. D. d’Enterria, Landolt-Bornstein **23**, 471 (2010)
2. U.A. Wiedemann, Landolt-Bornstein **23**, 521 (2010)
3. A. Accardi, F. Arleo, W.K. Brooks, D. d’Enterria, V. Muccifora, Riv. Nuovo Cim. **32**, 439 (2010)
4. A. Majumder, M. Van Leeuwen, Prog. Part. Nucl. Phys. **66**, 41 (2011)
5. I.M. Dremin, A.V. Leonidov, Phys. Usp. **53**, 1123 (2011)
6. Y. Mehtar-Tani, J.G. Milano, K. Tywoniuk, Int. J. Mod. Phys. A **28**, 1340013 (2013)
7. A. Majumder. [arXiv:1405.2019](https://arxiv.org/abs/1405.2019) [nucl-th]
8. I. Arsene et al. (BRAHMS Collaboration), Nucl. Phys. A **757**, 1 (2005)
9. B.B. Back et al. (PHOBOS Collaboration), Nucl. Phys. A **757**, 28 (2005)
10. J. Adams et al. (STAR Collaboration), Nucl. Phys. A **757**, 102 (2005)
11. K. Adcox et al. (PHENIX Collaboration), Nucl. Phys. A **757**, 184 (2005)
12. M. Spousta, Mod. Phys. Lett. A **28**, 1330017 (2013)

13. G. Aad et al. (ATLAS Collaboration), Phys. Rev. Lett. **105**, 252303 (2010)
14. S. Chatrchyan et al. (CMS Collaboration), Phys. Rev. C **84**, 024906 (2011)
15. S. Chatrchyan et al. (CMS Collaboration), Phys. Lett. B **712**, 176 (2012)
16. S. Chatrchyan et al. (CMS Collaboration), Phys. Lett. B **718**, 773 (2013)
17. G. Aad et al. (ATLAS Collaboration), Phys. Lett. B **719**, 220 (2013)
18. B. Abelev et al. (ALICE Collaboration), JHEP **1403**, 013 (2014)
19. G. Aad et al. (ATLAS Collaboration), Phys. Rev. Lett. **114**, 072302 (2015)
20. G. Aad et al. (ATLAS Collaboration), Phys. Rev. Lett. **111**, 152301 (2013)
21. S. Chatrchyan et al. (CMS Collaboration), Phys. Rev. Lett. **113**, 132301 (2014)
22. S. Chatrchyan et al. (CMS Collaboration), Eur. Phys. J. C **74**, 2951 (2014)
23. J. Casalderrey-Solana, J.G. Milhano, U.A. Wiedemann, J. Phys. G **8**, 035006 (2011)
24. G.-Y. Qin, B. Muller, Phys. Rev. Lett. **106**, 162302 (2011)
25. C. Young, B. Schenke, S. Jeon, C. Gale, Phys. Rev. C **84**, 024907 (2011)
26. D. Srivastava, J. Phys. G **38**, 055003 (2011)
27. I.P. Lokhtin, A.V. Belyaev, A.M. Snigirev, Eur. Phys. J. C **71**, 1650 (2011)
28. I.P. Lokhtin, A.V. Belyaev, L.V. Malinina, S.V. Petrushanko, E.P. Rogochaya, A.M. Snigirev, Eur. Phys. J. C **72**, 2045 (2012)
29. B. Betz, M. Gyulassy, Phys. Rev. C **86**, 024903 (2012)
30. T. Renk, Phys. Rev. C **85**, 064908 (2012)
31. T. Renk, Phys. Rev. C **86**, 061901 (2012)
32. T. Renk, Phys. Rev. C **88**, 014905 (2013)
33. L. Apolinario, N. Armesto, L. Cunqueiro, JHEP **1302**, 022 (2013)
34. K.C. Zapp, F. Krauss, U.A. Wiedemann, JHEP **1303**, 080 (2013)
35. W. Dai, I. Vitev, B.-W. Zhang, Phys. Rev. Lett. **110**, 142001 (2013)
36. J. Huang, Z.-B. Kang, I. Vitev, Phys. Lett. B **726**, 251 (2013)
37. B.G. Zakharov, JETP Lett. **96**, 616 (2013)
38. B.G. Zakharov, J. Phys. G **41**, 075008 (2014)
39. K.M. Burke et al., Phys. Rev. C **90**, 014909 (2014)
40. J. Xu, A. Buzzatti, M. Gyulassy, JHEP **1408**, 063 (2014)
41. Y. Mehtar-Tani, K. Tywoniuk, Phys. Lett. B **744**, 284 (2015)
42. J. Casalderrey-Solana, D.C. Gulhan, J.G. Milhano, D. Pablos, K. Rajagopal, JHEP **1410**, 19 (2014)
43. S. Chatrchyan et al. (CMS Collaboration), Phys. Lett. B **730**, 243 (2014)
44. S. Chatrchyan et al. (CMS Collaboration), Phys. Rev. C **90**, 024908 (2014)
45. G. Aad et al. (ATLAS Collaboration), Phys. Lett. B **739**, 320 (2014)
46. M. Cacciari, P. Quiroga-Arias, G.P. Salam, G. Soyez, Eur. Phys. J. C **73**, 2319 (2013)
47. I.P. Lokhtin, A.M. Snigirev, Eur. Phys. J. C **45**, 211 (2006)
48. T. Sjostrand, S. Mrenna, P. Skands, JHEP **0605**, 026 (2006)
49. R. Baier, YuL Dokshitzer, A.H. Mueller, S. Peigne, D. Schiff, Nucl. Phys. B **483**, 291 (1997)
50. R. Baier, YuL Dokshitzer, A.H. Mueller, D. Schiff, Phys. Rev. C **60**, 064902 (1999)
51. R. Baier, YuL Dokshitzer, A.H. Mueller, D. Schiff, Phys. Rev. C **64**, 057902 (2001)
52. YuL Dokshitzer, D. Kharzeev, Phys. Lett. B **519**, 199 (2001)
53. J.D. Bjorken, Fermilab publication Pub-82/29-THY (1982)
54. E. Braaten, M. Thoma, Phys. Rev. D **44**, 1298 (1991)
55. I.P. Lokhtin, A.M. Snigirev, Eur. Phys. J. C **16**, 527 (2000)
56. J.D. Bjorken, Phys. Rev. D **27**, 140 (1983)
57. J. Casalderrey-Solana, Y. Mehtar-Tani, C.A. Salgado, K. Tywoniuk, Phys. Lett. B **725**, 357 (2013)
58. R. Perez-Ramos, T. Renk, Phys. Rev. D **90**, 014018 (2014)
59. A. Kurkela, U.A. Wiedemann, Phys. Lett. B **740**, 172 (2015)
60. J.P. Blaizot, Y. Mehtar-Tani, M.A.C. Torres. [arXiv:1407.0326](https://arxiv.org/abs/1407.0326) [hep-ph]
61. I.P. Lokhtin, A.M. Snigirev, Phys. Lett. B **440**, 163 (1998)
62. Yu.L. Dokshitzer, V.A. Khoze, A.H. Mueller, S.I. Troian, *Basics of Perturbative QCD*, Frontieres edn. (Gif-sur-Yvette, 1991)
63. M. Cacciari, G.V. Salam, G. Soyez, JHEP **0804**, 063 (2008)
64. I.P. Lokhtin, A.M. Snigirev, Phys. Lett. B **567**, 39 (2003)
65. N. Armesto et al., J. Phys. G **35**, 054001 (2008)
66. D. Kharzeev, F. Loshaj, Phys. Rev. D **87**, 077501 (2013)
67. R. Perez-Ramos, T. Renk. [arXiv:1411.1983](https://arxiv.org/abs/1411.1983) [hep-ph]